First principles investigations of the optical selectivity of titanium carbide-based materials for concentrating solar power applications

W. Kim, Adel Mesbah, Xavier Deschanels, Samuel Bernard, S. Lebegue

Journal Name

ARTICLE TYPE

Cite this: DOI: 00.0000/xxxxxxxxxx

First principles investigations of the optical selectivity of titanium carbide-based materials for concentrating solar power applications†

Won June Kim,*[a,b] Adel Mesbah,[c] Xavier Deschanels,[d] Samuel Bernard,[e] and Sébastien Lebègue*[a]

Received Date
Accepted Date

DOI: 00.0000/xxxxxxxxxx

To improve the efficiency of concentrated solar power devices and to reach a high conversion rate of the solar energy into heat, a rational design of new high temperature absorber materials is a challenge of prime importance. Ultra-high temperature ceramics can fit the requirements to act as absorber materials, provided that their chemical composition and their properties are finely tuned. Within this context, we investigated the optical selectivity of titanium carbide modified with B, N, O impurity atoms or carbon vacancies, by first principles simulations. By computing the dielectric function and the reflectivity spectra of each composition, we found that modifying TiC can have important consequence on the optical properties of the bulk material, leading in certain cases to an enhancement of the optical selectivity. Then, we assess the performance of nanocomposites made of the corresponding nanoparticles embedded in a silicon carbide media by using Mie scattering theory fed by our ab initio dielectric functions. In this case, we found that while carbon vacancies are detrimental to selectivity, alloying TiC with boron improves notably the performance of the composite material, with an increase in selectivity of about 50 %.

1 Introduction

As the consideration about the global energy crisis and climate changes due to the use of fossil fuels increases, the development and use of efficient, renewable, and sustainable energy sources has become a great issue.[1] Among the various ways to solve such problems, solar energy is highly considered owing to the possibility that it offers for a massive generation of energy, for instance through concentrating solar power (CSP) technologies.[2,3] In CSP technologies, the sunlight is firstly concentrated on the absorber with the aid of several heliostats, followed by the conversion of the absorbed solar radiation into heat. Then, the converted heat is transferred into a fluid to operate the turbine of the power plant. Therefore, the design of an efficient absorber material is a key-point for a successful CSP technology, with the aim to maximize absorption of sunlight and to minimize infrared (IR) emittance at the same time. Furthermore, since the Carnot efficiency increases as the working temperature increases, therefore a high mechanical stability and resistance to oxidation are also required for good solar absorber materials.

In this regard, silicon carbide (SiC) has been commonly used as the absorber material due to its high absorptance and high resistance to oxidation up to 1400 °C. However, despite good sunlight absorption, SiC has a high thermal emittance, leading to a poor optical selectivity.[4,5] Thus, the main challenge is the development of novel absorber materials able to resist to damage at very high temperatures while keeping good spectral selectivity, good thermal conductivity and favorable radiative properties at the operating temperatures. Ultra-high temperature ceramics (UHTCs) could be the most appropriate candidates as solar absorber materials. UHTCs correspond to borides, carbides, and nitrides of transition metals in column IV, with particular chemical properties that show covalent and metallic characters simultaneously.[6] Because of this bonding character, UHTC materials show both a high reflectivity in the IR region and a high absorptance in the UV-vis-NIR region, and the resulting optical properties are therefore spectrally selective. Also, their covalent bonding leads to a

[a] Laboratoire de Physique et Chimie Théoriques LPCT (UMR CNRS 7019), Faculté des Sciences et Techniques, Université de Lorraine, BP70239, Boulevard des Aiguillettes, 54506 Vandoeuvre-lès-Nancy CEDEX, France. E-mail: sebastien.lebegue@univ-lorraine.fr

[b] Department of Biology and Chemistry, Changwon National University, Changwondaehak-ro 20, Uichang-gu, Changwon-si, 51140 Gyeongsangnam-do, South Korea. E-mail: wjkim@changwon.ac.kr

[c] Université Lyon 1, Institut de Recherches sur la Catalyse et l'Environnement de Lyon, IRCELYON, UMR5256, CNRS, 2 Avenue Albert Einstein, 69626, Villeurbanne Cedex, France.

[d] ICSM, Université de Montpellier, CEA, CNRS, ENSCM, Bagnols-sur-Cèze 30200, France.

[e] Univ. Limoges, CNRS, IRCER, UMR 7315, F-87000, Limoges, France.

† Electronic Supplementary Information (ESI) available: Comparison between calculated and experimental reflectivity of TiC. See DOI: 00.0000/00000000.

high melting temperature and makes them physically very stable. Among various UHTC materials, titanium carbide (TiC) is one of the most important compound. However, the major limitation of TiC is its low resistance to oxidation, therefore it usually required to protect it with a matrix while forming composite materials.[7] In particular, embedding TiC nanoparticles in a protective silicon carbide (SiC) matrix can compensate the limitations of the two materials as solar absorbers working at high temperature.

In spite of the many experimental studies on the optical properties of different UHTC materials and their nanocomposites, theoretical studies so far focused on the stability and electronic properties of such materials and their alloys.[8–22] To our knowledge, only few theoretical studies have been conducted to explore the optical properties of pure UHTC materials,[23–27] and there are no theoretical studies on the effect of alloying elements or impurities on their optical properties. In this paper, we study the optical properties of TiC and the effect of alloying elements B, N, O or carbon vacancy using first principles calculations. Our choice is motivated by the fact that TiC has a strong tendency to form non stoichiometric compositions,[28] while B, N, and O atoms have a size close to the one of carbon, and therefore upon alloying the crystal structure of TiC will be mostly preserved. We searched various compositions based on TiC up to four-component alloy systems, then assessed their performance for CSP absorbers by investigating their reflectivity spectra. Then, to be as close as possible to experimental conditions, we studied their spectral selectivity when they are embedded as nanoparticles in a SiC substrate.

2 Computational Details

Our calculations have been performed using density functional theory (DFT) with the projector augmented wave method as implemented in the Vienna ab initio simulation package (VASP),[29,30] except for the calculation of the electron-phonon interaction part of the electron scattering rate (see below). The generalized gradient approximation (GGA) designed by Perdew, Burke, and Ernzerhof (PBE) was used for the exchange-correlation functional,[31] and an energy cutoff of 550 eV was chosen for the the plane wave basis set. The electronic total energy has been converged until the total energy difference between electronic steps became smaller than a threshold of 10^{-7} eV, and a geometry optimization was performed until all atomic forces became smaller than 5.0×10^{-3} eV/Å. For the geometry relaxation, we used a Γ-centered **k**-mesh with a grid step of 0.2 Å^{-1}, which corresponds to $13\times13\times13$ and $7\times7\times7$ **k**-points for the primitive cell of TiC and its $2\times2\times2$ supercell, respectively.

Experimentally, it has been shown that carbon vacancies[28,32] or the incorporation of other 2p-block elements[32–35] can be realized in TiC. Following these facts, our structural models have been designed using the following procedure: firstly, we obtained the equilibrium lattice parameter of TiC with the rock-salt structure (space group No. 225, $Fm\bar{3}m$). Our calculated lattice parameter $a=4.33$ Å is close to the experimental value of 4.329 Å.[36] Then to study the effect of alloying elements on the optical properties of TiC, we constructed a $2\times2\times2$ supercell to model the following systems: 1) singly doped systems (see Figure 1(a)) in which one carbon atom is replaced with a vacancy (V_C) or a B, N, or O atom,

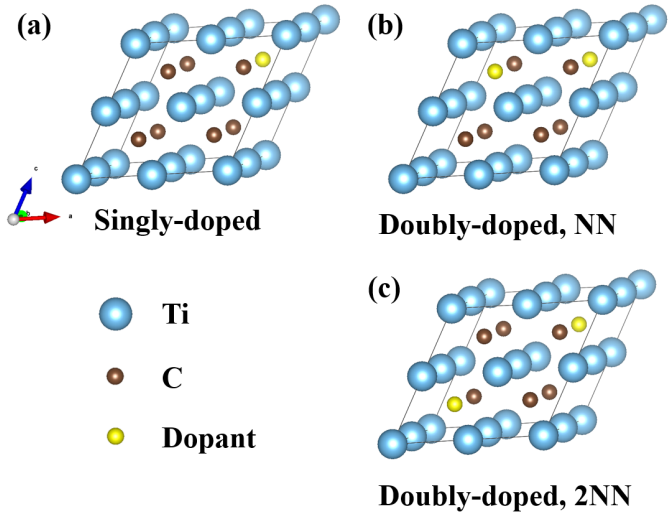

Fig. 1 Atomic structures of (a) singly and (b) doubly doped configurations of TiC used in the present study.

and 2) doubly doped systems (see Figure 1(b)) in which two carbon atoms are replaced by V_C-V_C, B-B, N-N, O-O, V_C-B, V_C-N, V_C-O, B-N, B-O, or N-O pairs of atoms. For the doubly doped systems, when considering the crystal symmetry of TiC, there are only two possible configuration for the dopants: nearest neighbor (NN) or next nearest neighbor (2NN), respectively. We relaxed the two possible geometries for each system, and then the most stable configuration was selected for the calculation of the optical properties.

To study the optical properties of TiC and its alloys, we calculated the frequency dependent dielectric function, $\varepsilon(\omega)=\varepsilon^{(1)}(\omega)+i\varepsilon^{(2)}(\omega)$. For metallic systems, the total dielectric function can be divided into interband and intraband terms, $\varepsilon(\omega)=\varepsilon^{\text{inter}}(\omega)+\varepsilon^{\text{intra}}(\omega)$. The first term is written in the independent particle approximation (IPA) and in the limit of long wavelength as:

$$\varepsilon^{(2),\text{inter}}_{\alpha\beta}(\omega)=\frac{4\pi^2e^2}{\Omega}\lim_{q\to0}\frac{1}{q^2}\sum_{c,v,\mathbf{k}}2w_{\mathbf{k}}\delta\left(E_{c\mathbf{k}}-E_{v\mathbf{k}}-\omega\right)\times\langle u_{c\mathbf{k}+\mathbf{e}_\alpha q}|u_{v\mathbf{k}}\rangle\langle u_{v\mathbf{k}}|u_{c\mathbf{k}+\mathbf{e}_\beta q}\rangle \quad (1)$$

where e is the electron charge, Ω is the cell volume, $w_{\mathbf{k}}$ is the weight of the **k**-points, $\mathbf{e}_i$ is a unit vector in cartesian coordinates, and c and v are the indices for the conduction and valence states, whereas $u_{j\mathbf{k}}$ and $E_{j\mathbf{k}}$ are the one-electron Blöch functions and eigenvalues, respectively. Then we can apply a Kramers–Kronig relation to calculate the real part, $\varepsilon^{(1),\text{inter}}(\omega)$, by using:

$$\varepsilon^{(1),\text{inter}}_{\alpha\beta}(\omega)=1+\frac{2}{\pi}P\int_0^\infty\frac{\varepsilon^{(2),\text{inter}}(\omega')\omega'}{\omega'^2-\omega^2+i\eta}d\omega' \quad (2)$$

where P is the principal value and η is an infinitesimal complex shift. It is noteworthy to mention that our calculated dielectric function could be affected by the level of theory used, within DFT or beyond, like with the GW approximation. Here, the metallic nature of TiC makes the effect of the self-energy correction

on optical properties negligible, with a GW density of states very close to the one obtained with GGA (data not shown here). A similar finding has been made by M. Kumar et al.[26], for Au and TiN. Therefore, all the dielectric functions in this study have been calculated within the GGA formalism.

For the intraband contribution to the dielectric function, we employed the Drude expression:[26,37,38] for a given plasma frequency, ω_p, and a scattering rate, γ, $\varepsilon^{\text{intra}}(\omega)$ can be approximated by the following equation:

$$\varepsilon^{\text{intra}}(\omega) = 1 - \frac{\omega_p^2}{\omega^2 + i\gamma\omega} \tag{3}$$

where the plasma frequency can be obtained from the electronic structure by tracing the following tensor:[38]

$$\omega_{p,\alpha\beta}^2 = -\frac{4\pi e^2}{\Omega}\sum_{v,\mathbf{k}} 2\frac{\partial w_{\mathbf{k}}(E_v)}{\partial E_v}\left(\frac{\partial E_{v\mathbf{k}}}{\partial \mathbf{k}}\mathbf{e}_\alpha\right)\left(\frac{\partial E_{v\mathbf{k}}}{\partial \mathbf{k}}\mathbf{e}_\beta\right) \tag{4}$$

The second parameter, the electron scattering rate, can be calculated from the imaginary part of the electron-phonon self-energy, $\Sigma_{n\mathbf{k}}(T)$.[27,38,39] From the electronic band structure and phonon dispersion, the self-energy is expressed as:[40]

$$\Sigma_{n\mathbf{k}}(T) = \frac{2\pi}{\hbar}\sum_{\mathbf{q}\nu,m} w_{\mathbf{q}}|g^{SE}_{mn,\nu}(\mathbf{k},\mathbf{q})|^2 \times\left[\frac{n_{\mathbf{q}\nu}(T)+f_{m\mathbf{k}+\mathbf{q}}(T)}{E_{n\mathbf{k}}-E_{m\mathbf{k}'}+\omega_{\mathbf{q}\nu}-i\eta}+\frac{n_{\mathbf{q}\nu}(T)+1+f_{m\mathbf{k}+\mathbf{q}}(T)}{E_{n\mathbf{k}}-E_{m\mathbf{k}'}-\omega_{\mathbf{q}\nu}-i\eta}\right] \tag{5}$$

where $\omega_{\mathbf{q}\nu}$ is the phonon frequency of branch ν and wave vector $\mathbf{q}$, $n_{\mathbf{q}\nu}(T)$ is the Bose-Einstein distribution, and $f_{m\mathbf{k}+\mathbf{q}}(T)$ is the Fermi-Dirac distribution. $g^{SE}_{mn,\nu}(\mathbf{k},\mathbf{q})$ is the electron-phonon matrix element. Then the scattering rate of electron in the band n and wave vector $\mathbf{k}$ is given by $\gamma_{ep}(n\mathbf{k},T) = 2\text{Im}\Sigma_{n\mathbf{k}}(T)$. For the calculation of the dielectric function, we averaged $\gamma_{ep}(n\mathbf{k},T)$ over the Fermi surface as follows:[41,42]

$$\gamma_{ep}(T) = \int_{-\infty}^{+\infty}\gamma_{ep}(\varepsilon,T)\left(-\frac{\partial f}{\partial \varepsilon}\right)d\varepsilon \tag{6}$$

where $\gamma_{ep}(\varepsilon,T)$ is the energy-dependent scattering rate obtained by integrating $\gamma_{ep}(n\mathbf{k},T)$ over the first Brillouin zone.

An other contribution to the electron scattering rate is due to electron-electron scattering, which can be modeled from the self-energy in the GW approximation. In the study of M. Xu el al.,[38] the effect of electron-electron scattering rate on the total dielectric functions of noble metals (Au, Ag, and Cu) has been shown to be negligible. Likewise, our test showed that the contribution of the electron-electron scattering rate in pure TiC is also small. Therefore, we neglected this contribution in the calculations of the other compounds.

The calculation of the electron-phonon interaction has been done by using the Quantum Espresso code[43,44] and the EPW[40,45] package. The plane waves were expanded up to a kinetic energy of 70 Ry, and the same $\mathbf{k}$-grid as in the VASP calculations was used for the self-consistent calculations. The phonon dispersion has been obtained with a $3\times3\times3$ $\mathbf{q}$-grid, then the electron-phonon coupling has been calculated with a finer BZ sampling ($12\times12\times12$ $\mathbf{k}$-points and $20\times20\times20$ $\mathbf{q}$-points) through a Wannier functions representation.

Table 1 Configuration, plasma frequencies, scattering rate, and crossover frequency of TiC and its alloys.

Composition	Configuration	ω_p (eV)	γ_{ep} (meV)	ω_c (eV)
Ti_8C_8	-	3.55	17.09	0.70
Ti_8C_7	-	2.22	26.34	0.31
Ti_8C_7B	-	3.93	31.24	1.11
Ti_8C_7N	-	3.99	28.74	0.90
Ti_8C_7O	-	4.43	45.91	1.11
Ti_8C_6	NN	3.38	54.86	0.79
$Ti_8C_6B_2$	NN	4.88	35.71	1.21
$Ti_8C_6N_2$	2NN	4.63	48.85	1.14
$Ti_8C_6O_2$	NN	4.71	51.42	1.54
Ti_8C_6B	NN	3.45	41.51	0.72
Ti_8C_6N	NN	3.37	57.01	0.54
Ti_8C_6O	NN	3.40	53.20	0.93
Ti_8C_6BN	NN	2.92	23.80	0.70
Ti_8C_6BO	NN	3.64	28.25	0.95
Ti_8C_6NO	NN	4.70	52.66	1.36

3 Results and Discussion

3.1 Bulk electronic and dielectric properties

Table 1 shows our calculated plasma frequencies and scattering rates for TiC and its alloys. The plasma frequency of pure TiC is 3.55 eV, which is similar to the previous result of Kumar et al.[26] Compared with pure TiC, the compounds with a carbon vacancy (V_C), i.e., Ti_8C_7, Ti_8C_6 and Ti_8C_6X (X = B, N, O) show smaller ω_p values due to the deficiency of electrons. On the other hand, there are two behaviors when the carbon atoms are substituted with other elements without a vacancy: the plasma frequencies of Ti_8C_7X and $Ti_8C_6X_2$ are larger than the one of pure TiC, whereas the substitution of two different elements (BN, BO, and NO pairs) does not present a systematic trend. For singly-doped systems, the plasma frequency increases as the number of electrons increases, i.e., from Ti_8C_7B to Ti_8C_7O. For doubly-doped systems with different dopants, the same trend is seen with ω_p increasing from BN to BO and NO. Concerning the scattering rates, it is seen from our results that they are always larger for the alloys than for pure TiC, a fact that can be intuitively understood by the increased disorder in the alloys in comparison with the perfect TiC crystal.

Using the parameters presented in table 1 and the interband contribution of the dielectric function, we calculated the total dielectric function for the whole set of compounds investigated here, the results being presented in Figure 2. Among the compositions that we studied, the dielectric functions of pure TiC and (V_C)-containing TiC compares well with available experimental data: for instance, Pflüger and co-workers have measured the bulk dielectric function of stoichiometric TiC by electron-energy-loss spectroscopy (EELS).[46] Also, Koide and co-workers studied the effect of the concentration of (V_C) on the dielectric properties of TiC.[28] Here, Ti_8C_6 has a vacancy concentration close to the $TiC_{0.6}$ sample of their work.

In terms of the optical selectivity of the photothermal absorber, an important parameter is the frequency where the total reflec-

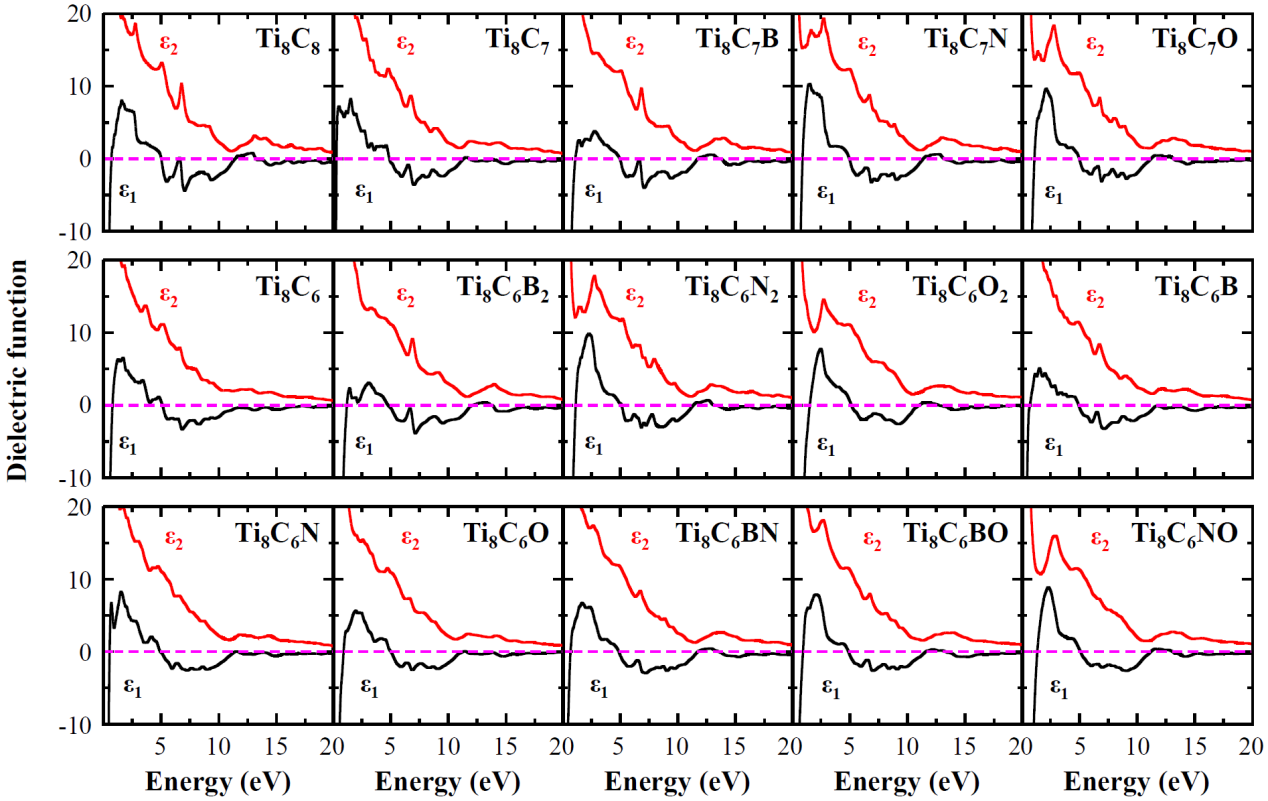

Fig. 2 Calculated total dielectric functions of TiC and its alloys. The black and red solid lines correspond to the real and imaginary parts of the dielectric function, respectively. The magenta dashed line is to guide to the eyes corresponding to zero.

tion turns off. To figure this out, we investigated the crossover frequency, ω_c, at which the real part of the dielectric function crosses zero for the first time. The last column of table 1 shows the value of ω_c for each system. The crossover frequency of pure TiC, 0.70 eV, is in good agreement with the value (0.68 eV) of Kumar et al.[26] By comparing with pure TiC, the effect of alloying can be classified following three patterns. Firstly, when one or two carbon vacancies are introduced, the crossover frequency is either decreased or stable, with Ti_8C_6O, which has a value of ω_c of 0.93 eV, being an exception. Secondly, the crossover frequency is increased when the carbon atoms are substituted by an other single type of element (Ti_8C_7X and $Ti_8C_6X_2$), with a larger increase of ω_c by doping with B or O than with N. The last case is when doping with two different elements, the crossover frequency increases in the order BN < BO < NO, following the trends of both the plasma frequency and the scattering rate.

Figure 3 shows our calculated reflectivity spectra for TiC and its alloys, with the frequency-dependent reflectivity calculated as :

$$R(\omega) = \left| \frac{\varepsilon^{1/2}(\omega) - 1}{\varepsilon^{1/2}(\omega) + 1} \right|^2 \quad (7)$$

Henning and Mutschke have measured the reflectivity spectrum of bulk TiC using infrared reflectivity spectroscopy.[47] More recently, Aréna and co-workers conducted more elaborate measurements of the reflectivity spectra, as varying the relative density of the TiC sample.[48] Our calculated reflectivity spectrum of TiC shows a good agreement with their experimental data (See figure S1 in the ESI† for direct comparison.). For photothermal applications, an optimal selectivity at room temperature (which is the temperature at which our phonons calculations were conducted) is obtained when a relatively sharp drop of the reflectivity at around 2.5 μm is observed.[1] While certain systems (Ti_8C_6, Ti_8C_6B, Ti_8C_6N, or Ti_8C_6O) show a reflectivity in the IR region which is roughly similar to the one of TiC, for Ti_8C_7 and Ti_8C_6BN) it appears to be significantly lower. However, for Ti_8C_7B, and Ti_8C_6BO a small increase of the reflectivity around $\lambda = 2.5$ μm can be observed, while for the remaining compounds (Ti_8C_7N, Ti_8C_7O, $Ti_8C_6B_2$, $Ti_8C_6N_2$, $Ti_8C_6O_2$, and Ti_8C_6NO), the changes are more drastic, with either a displacement of the transition towards shorter wavelengths and/or an increased value of the IR reflectivity, showing that a modification of TiC can affect significantly its reflectivity.

3.2 Optical properties of nanoparticles

For applications in concentrating solar power (CSP) units, transition metal carbides are usually included in the form of nanoparticles in a matrix, such as SiC.[48,49] Since such systems cannot be directly investigated using density functional theory for computational reasons, we have investigated the optical properties of the nanoparticles using the scattering theory of Mie,[50,51] which we outline briefly below. When the size a of a nanoparticle is comparably smaller than the wavelength of the incident light λ, Mie theory states that the extinction, scattering, and absorption cross

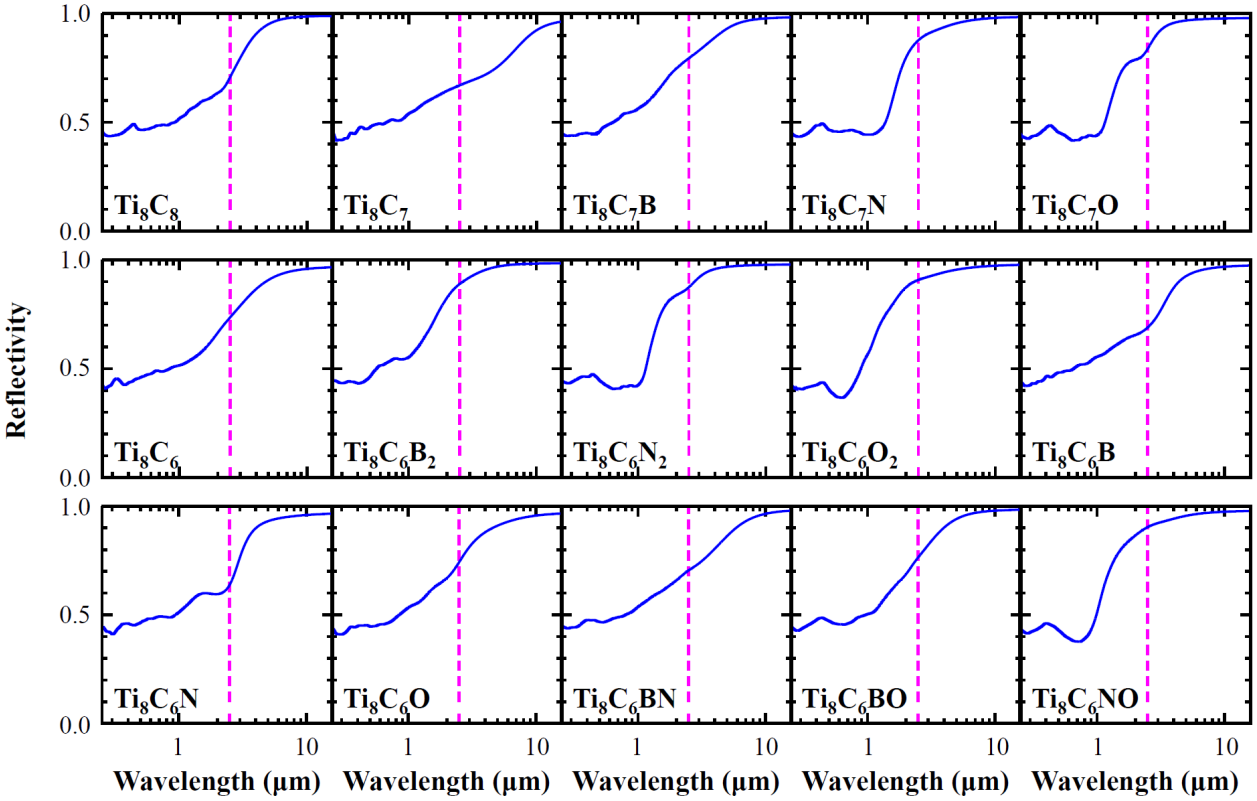

Fig. 3 Calculated reflectivity spectra of TiC and its alloys, as a function of wavelength. The magenta dashed line in each plot is the wavelength where the reflectivity should turn off for an ideal photothermal absorber (λ = 2.5 μm.)

sections (Q_{ext}, Q_{sca}, and Q_{abs}, respectively) of this particle can be calculated using the following equations:

$$Q_{\text{ext}} = \frac{2}{x^2}\sum_{L=1}^{\infty}(2L+1)\,\text{Re}\left[a_L + b_L\right] \tag{8}$$

$$Q_{\text{sca}} = \frac{2}{x^2}\sum_{L=1}^{\infty}(2L+1)\left(|a_L|^2 + |b_L|^2\right) \tag{9}$$

$$Q_{\text{abs}} = Q_{\text{ext}} - Q_{\text{sca}} \tag{10}$$

In the equations above, the coefficients a_L and b_L are written by using spherical Riccati-Bessel functions Ψ_L and ξ_L and their derivatives:

$$a_L = \frac{m\Psi_L(mx)\Psi_L'(x) - \Psi_L(x)\Psi_L'(mx)}{m\Psi_L(mx)\xi_L'(x) - \xi_L(x)\Psi_L'(mx)} \tag{11}$$

$$b_L = \frac{\Psi_L(mx)\Psi_L'(x) - m\Psi_L(x)\Psi_L'(mx)}{\Psi_L(mx)\xi_L'(x) - m\xi_L(x)\Psi_L'(mx)} \tag{12}$$

where $x = 2\pi a/\lambda$ is the reduced particle size and $m = n_{\text{met}}/n_{\text{die}}$ is the ratio between the refraction index of the nanoparticle and that of the surrounding dielectric media. With the help of the package PyMieScatt,[52] the scattering and absorption cross section, Q_{sca} and Q_{abs}, have been calculated by using the complex refractive index obtained form the dielectric function presented earlier in figure 2. For the host material surrounding the nanoparticle, we set $\varepsilon_\infty = 2.63$, which corresponds to SiC. The diameter of the nanoparticles was set to 50 nm.

Figure 4 shows our calculated scattering and absorption cross section of nanoparticles of TiC and its alloys. Comparing with the reflectivity spectra in figure 3, two patterns are observed in the behavior of Q_{abs}. Firstly, if the reflectivity increases slowly, as in pure TiC, Q_{abs} has only one peak below 1 μm. Ti_8C_6BN and the systems with a C-vacancy (except for Ti_8C_6N) show this behavior. On the other hand, if the reflectivity decreases rapidly, there is a second peak between 1 μm and 2.5 μm. This second peak is observed when nitrogen or oxygen (or both of them) is present in the composition. Some systems, including boron-doped compositions and Ti_8C_6N, show an intermediate behavior: only a small shoulder appears after the first peak. In terms of reflectivity, this behavior is related to the small increase of the reflectivity in the IR region compared to that of pure TiC.

The selectivity of the different compounds can be directly accessed if we use a parameter that can quantify the absorbance in the UV/visible versus the absorbance in the IR region. This can be achieved by integrating Q_{abs}, weighted by either the solar and or blackbody intensities as:

$$I_{\text{abs}}^{\text{solar}} = \int_{\lambda_1}^{\lambda_2} Q_{\text{abs}}(\lambda)P(\lambda)\,d\lambda \tag{13}$$

$$I_{\text{abs}}^{\text{BB}} = \int_{\lambda_1}^{\lambda_2} Q_{\text{abs}}(\lambda)B(\lambda)\,d\lambda \tag{14}$$

where $P(\lambda)$ and $B(\lambda)$ are the solar and blackbody spectrum, respectively. To cover both the UV/visible and IR regions, the in-

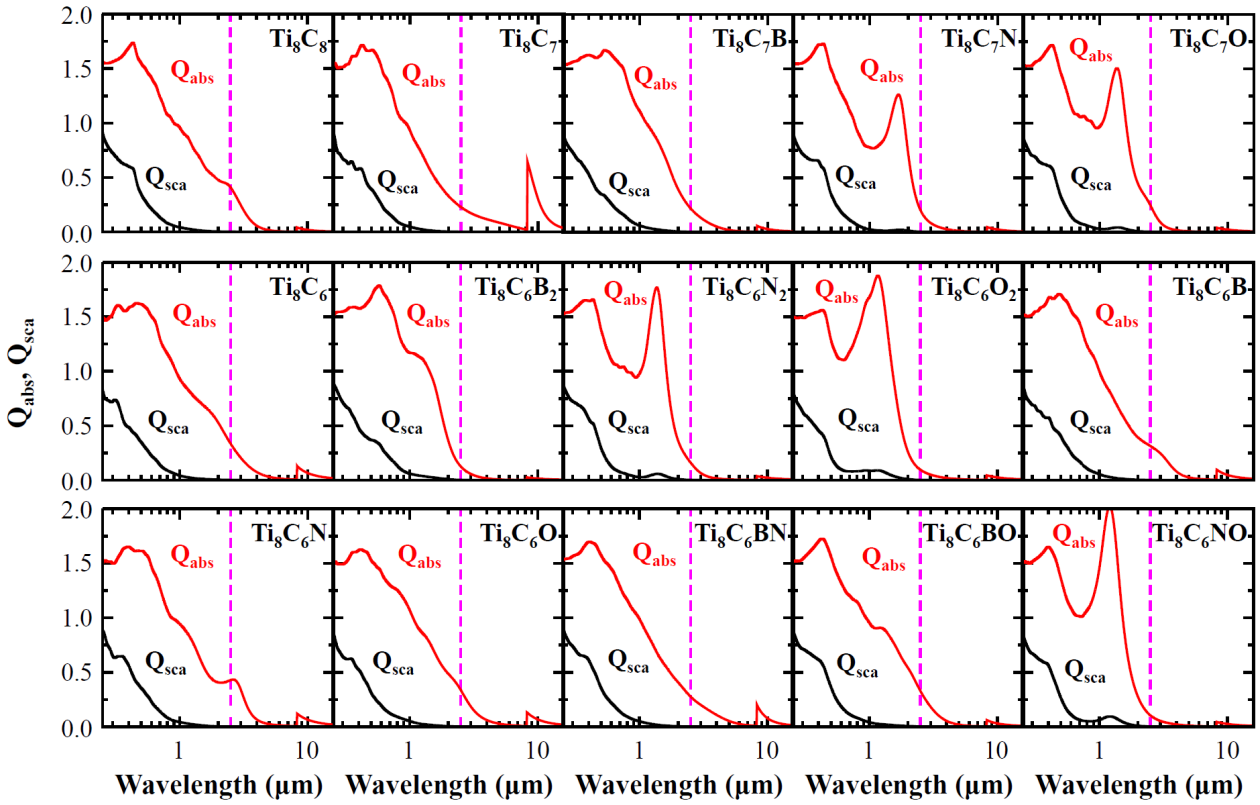

Fig. 4 Q_{abs} (red solid lines) and Q_{sca} (black solid lines) spectra for a 50 nm nanoparticle of TiC-based compound embedded in a SiC matrix. The magenta dashed line in each plot has the same meaning as in the Figure 3

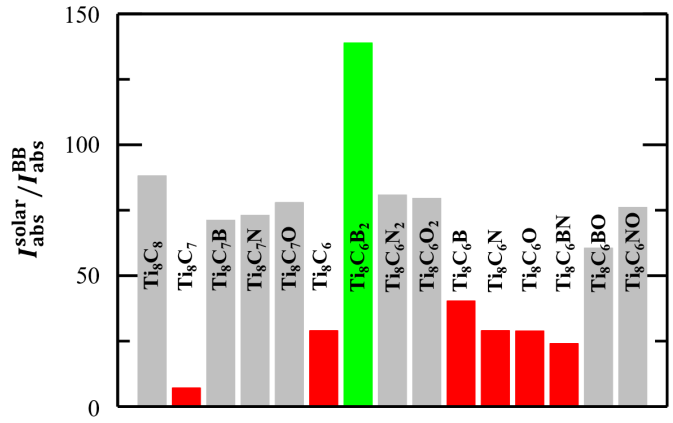

Fig. 5 Values of $I_{abs}^{solar}/I_{abs}^{BB}$ for different TiC-based nanoparticles embedded in SiC matrix at 300 K.

tegration has been done for a range between 0.28 and 16 μm, and with a blackbody temperature of $T = 300$ K, which corresponds mostly to infrared radiations. Then, a large $I_{abs}^{solar}/I_{abs}^{BB}$ will correspond to a high selectivity .

Figure 5 shows $I_{abs}^{solar}/I_{abs}^{BB}$ for TiC and its alloys in the form of nanoparticles. Compared with pure TiC, the alloys containing carbon vacancies as well as Ti_8C_6BN show a very low optical selectivity. This is due to two factors: 1) a lower value of the maximum of Q_{abs} compared to TiC and 2) a more smeared Q_{abs} above 2.5 μm compared to TiC (see figure 4). While most of the substituted alloys shows a selectivity similar to that of TiC, $Ti_8C_6B_2$ shows a noticeably larger selectivity. In this case, Q_{abs} is on the overall larger than for TiC in the UV/visible region ($\lambda < 2.5$ μm), and also shows very small area in the IR region ($\lambda > 2.5$ μm). These facts leads to both a larger UV/visible absorbance and a lower IR emission, making the composition $Ti_8C_6B_2$ the best candidate for a photothermal absorber material among the formulations that we have investigated, with a selectivity which is roughly 50 % better than the one of TiC.

4 Conclusion

In this work, we have studied the effect of doping on the optical properties of TiC using first principles calculations. By substituting carbon by B, N, O atoms or by introducing a carbon vacancy, we calculated the dielectric function and reflectivity spectra of TiC and its alloys in the bulk phase. For the 15 different compositions of TiC and its alloys, the crossover frequency for the real part of dielectric function is highly related to the transition of reflectivity near $\lambda = 2.5$ μm, at which the reflectivity should be truned off for the ideal photothermal absorbers; the higher the crossover frequency is, the better the reflectivity behavior is. From this analysis, we found that the IR reflectivity decreases when the carbon vacancy is introduced.

Then, the overall performance of the different compounds has been accessed through Mie scattering theory by simulating the properties of the corresponding nanoparticles embedded in a SiC

host. It was shown that while carbon vacancies are detrimental to the selectivty of the material, the $Ti_8C_6B_2$ composition shows a selectivity which is 50 % larger than the one of TiC, a fact which is promising in the aim of increasing the efficiency of concentrating solar power devices, and can serve as a guideline for future experimental studies in this field.

Author contributions

W.J.K. carried out the calculations. W.J.K. and S. L wrote the first version of the manuscript. All authors discussed the results and contributed to the final manuscript.

Conflicts of interest

There are no conflicts to declare.

Acknowledgements

The authors acknowledge financial support from the Agence Nationale de la Recherche within the CARAPASS ("Carbide & Carbonitride nanocomposite based photothermal solar absorbers") project (Grant No. ANR-16-CE08-0026).

Notes and references

1 K. Xu, M. Du, L. Hao, J. Mi, Q. Yu and S. Li, *J. Materiomics*, 2020, **6**, 167–182.
2 C. Granqvist, *Adv. Mater.*, 2003, **15**, 1789–1803.
3 Y. Tian and C. Zhao, *Applied Energy*, 2013, **104**, 538–553.
4 C. Agrafiotis, I. Mavroidis, A. Konstandopoulos, B. Hoffschmidt, P. Stobbe, M. Romero and V. Fernandezquero, *Sol. Energy Mater. Sol. Cells*, 2007, **91**, 474–488.
5 S. Mey, C. Caliot, G. Flamant, A. Kribus and Y. Gray, *Energy Procedia*, 2014, **49**, 478–487.
6 E. Sani, L. Mercatelli, D. Jafrancesco, J. L. Sans and D. Sciti, *J. Europ. Opt. Soc. Rap. Public.*, 2012, **7**, 12052.
7 E. Ionescu, S. Bernard, R. Lucas, P. Kroll, S. Ushakov, A. Navrotsky and R. Riedel, *Adv. Eng. Mater.*, 2019, **21**, 1900269.
8 K. Kobayashi, *Surf. Sci.*, 2001, **493**, 665–670.
9 Z. Dridi, B. Bouhafs, P. Ruterana and H. Aourag, *J. Phys.: Condens. Matter*, 2002, **14**, 10237–10249.
10 Z. Wu, X.-J. Chen, V. V. Struzhkin and R. E. Cohen, *Phys. Rev. B*, 2005, **71**, 214103.
11 A. Zaoui, B. Bouhafs and P. Ruterana, *Mater. Chem. and Phys.*, 2005, **91**, 108–115.
12 E. I. Isaev, S. I. Simak, I. A. Abrikosov, R. Ahuja, Y. K. Vekilov, M. I. Katsnelson, A. I. Lichtenstein and B. Johansson, *J. of Appl. Phys.*, 2007, **101**, 123519.
13 O. Adjaoud, G. Steinle-Neumann, B. P. Burton and A. van de Walle, *Phys. Rev. B*, 2009, **80**, 134112.
14 Z. Gao and S. Kang, *Solid State Commun.*, 2013, **156**, 25–30.
15 Q. Zeng, J. Peng, A. R. Oganov, Q. Zhu, C. Xie, X. Zhang, D. Dong, L. Zhang and L. Cheng, *Phys. Rev. B*, 2013, **88**, 214107.
16 Y. Liu, Y. Jiang, R. Zhou and J. Feng, *J. Alloys Compd.*, 2014, **582**, 500–504.
17 D. Y. Dang, J. L. Fan and H. R. Gong, *J. of Appl. Phys.*, 2014, **116**, 033509.
18 S. Yu, Q. Zeng, A. R. Oganov, G. Frapper and L. Zhang, *Phys. Chem. Chem. Phys.*, 2015, **17**, 11763–11769.
19 S. Yu, Q. Zeng, A. R. Oganov, G. Frapper, B. Huang, H. Niu and L. Zhang, *RSC Adv.*, 2017, **7**, 4697–4703.
20 L. Chen, Q. Wang, L. Xiong and H. Gong, *J. Alloys Compd.*, 2018, **747**, 972–977.
21 X. Fan, S. Wang, X. Yang, G. Ni, J. Zhang and D. Li, *J. Mater. Res.*, 2018, **33**, 1650–1658.
22 N. Mediukh, V. Ivashchenko, P. Turchi, V. Shevchenko, J. Leszczynski and L. Gorb, *Calphad*, 2019, **66**, 101643.
23 A. Delin, O. Eriksson, R. Ahuja, B. Johansson, M. S. S. Brooks, T. Gasche, S. Auluck and J. M. Wills, *Phys. Rev. B*, 1996, **54**, 1673–1681.
24 J. Kim, S.-H. Jhi and K. Ryeol Lee, *J. of Appl. Phys.*, 2011, **110**, 083501.
25 F. Mehmood, R. Pachter, N. R. Murphy and W. E. Johnson, *J. Appl. Phys.*, 2015, **118**, 195302.
26 M. Kumar, N. Umezawa, S. Ishii and T. Nagao, *ACS Photonics*, 2016, **3**, 43–50.
27 A. Habib, F. Florio and R. Sundararaman, *J. Opt.*, 2018, **20**, 064001.
28 T. Koide, T. Shidara, H. Fukutani, A. Fujimori, T. Miyahara, H. Kato, S. Otani and Y. Ishizawa, *Phys. Rev. B*, 1990, **42**, 4979–4995.
29 G. Kresse and J. Furthmüller, *Phys. Rev. B*, 1996, **54**, 11169–11186.
30 G. Kresse and D. Joubert, *Phys. Rev. B*, 1999, **59**, 1758–1775.
31 J. P. Perdew, K. Burke and M. Ernzerhof, *Phys. Rev. Lett.*, 1996, **77**, 3865–3868.
32 E. Amberger and H. P. Gerster, *Acta Cryst. B*, 1980, **36**, 672–675.
33 H. Duschanek, P. Rogl and H. L. Lukas, *J. Phase Equilibra*, 1995, **16**, 46–60.
34 P. Ettmayer, H. Kolaska, W. Lengauer and K. Dreyer, *Int. J. Refract. Metals Hard Mater.*, 1995, **13**, 343–351.
35 C. L. Yeh and Y. D. Chen, *Ceram. Int.*, 2005, **31**, 719–729.
36 A. Dunand, H. D. Flack and K. Yvon, *Phys. Rev. B*, 1985, **31**, 2299–2315.
37 H. Ehrenreich and H. R. Philipp, *Phys. Rev.*, 1962, **128**, 1622–1629.
38 M. Xu, J.-Y. Yang, S. Zhang and L. Liu, *Phys. Rev. B*, 2017, **96**, 115154.
39 M. Bernardi, J. Mustafa, J. B. Neaton and S. G. Louie, *Nat Commun.*, 2015, **6**, 7044.
40 S. Poncé, E. Margine, C. Verdi and F. Giustino, *Comput. Phys. Commun.*, 2016, **209**, 116–133.
41 G. R. Parkins, W. E. Lawrence and R. W. Christy, *Phys. Rev. B*, 1981, **23**, 6408–6416.
42 J. I. Mustafa, M. Bernardi, J. B. Neaton and S. G. Louie, *Phys. Rev. B*, 2016, **94**, 155105.
43 P. Giannozzi, S. Baroni, N. Bonini, M. Calandra, R. Car, C. Cavazzoni, D. Ceresoli, G. L. Chiarotti, M. Cococ-

cioni, I. Dabo, A. Dal Corso, S. de Gironcoli, S. Fabris, G. Fratesi, R. Gebauer, U. Gerstmann, C. Gougoussis, A. Kokalj, M. Lazzeri, L. Martin-Samos, N. Marzari, F. Mauri, R. Mazzarello, S. Paolini, A. Pasquarello, L. Paulatto, C. Sbraccia, S. Scandolo, G. Sclauzero, A. P. Seitsonen, A. Smogunov, P. Umari and R. M. Wentzcovitch, *J. Phys.: Condens. Matter*, 2009, **21**, 395502.

44 P. Giannozzi, O. Andreussi, T. Brumme, O. Bunau, M. Buongiorno Nardelli, M. Calandra, R. Car, C. Cavazzoni, D. Ceresoli, M. Cococcioni, N. Colonna, I. Carnimeo, A. Dal Corso, S. de Gironcoli, P. Delugas, R. A. DiStasio, A. Ferretti, A. Floris, G. Fratesi, G. Fugallo, R. Gebauer, U. Gerstmann, F. Giustino, T. Gorni, J. Jia, M. Kawamura, H.-Y. Ko, A. Kokalj, E. Küçükbenli, M. Lazzeri, M. Marsili, N. Marzari, F. Mauri, N. L. Nguyen, H.-V. Nguyen, A. Otero-de-la Roza, L. Paulatto, S. Poncé, D. Rocca, R. Sabatini, B. Santra, M. Schlipf, A. P. Seitsonen, A. Smogunov, I. Timrov, T. Thonhauser, P. Umari, N. Vast, X. Wu and S. Baroni, *J. Phys.: Condens. Matter*, 2017, **29**, 465901.

45 J. Noffsinger, F. Giustino, B. D. Malone, C.-H. Park, S. G. Louie and M. L. Cohen, *Computer Physics Communications*, 2010, **181**, 2140–2148.

46 J. Pflüger, J. Fink, W. Weber, K. P. Bohnen and G. Crecelius, *Phys. Rev. B*, 1984, **30**, 1155–1163.

47 T. Henning and H. Mutschke, *Spectrochim. Acta A: Mol. Biomol. Spectrosc.*, 2001, **57**, 815–824.

48 H. Aréna, M. Coulibaly, A. Soum-Glaude, A. Jonchère, A. Mesbah, G. Arrachart, N. Pradeilles, M. Vandenhende, A. Maitre and X. Deschanels, *Sol. Energy Mater. Sol. Cells*, 2019, **191**, 199–208.

49 H. Aréna, M. Coulibaly, A. Soum-Glaude, A. Jonchère, G. Arrachart, A. Mesbah, N. Pradeilles, M. Vandenhende, A. Maître and X. Deschanels, *Sol. Energy Mater. Sol. Cells*, 2020, **213**, 110536.

50 G. Mie, *Ann. Phys.*, 1908, **330**, 377–445.

51 C. F. Bohren and D. R. Huffman, *Absorption and scattering of light by small particles*, Wiley, New York, NY, 1983.

52 B. J. Sumlin, W. R. Heinson and R. K. Chakrabarty, *J. Quant. Spectrosc. Radiat. Transf.*, 2018, **205**, 127–134.